Supplementary information

Electrochemical fabrication of multiple crystalline-amorphous heterogeneous single-atom electrocatalysts for alkaline oxygen evolution reaction

Qi Zhang,[a] Peiyao Pan,[a] Xuewen Xia,[a] Shujuan Wang,[b] Zhongya Pang,[a] Guangshi Li,[a] Li Ji,[c] Xing Yu,*[a] Xionggang Lu[ad] and Xingli Zou*[a]

[a]*State Key Laboratory of Advanced Special Steel & Shanghai Key Laboratory of Advanced Ferrometallurgy & School of Materials Science and Engineering, Shanghai University, Shanghai 200444, China*

[b]*Shanghai Institute of Applied Physics, Chinese Academy of Sciences, Shanghai 201800, China.*

[c]*State Key Laboratory of ASIC and System, School of Microelectronics, Fudan University, Shanghai 200433, China*

[d]*School of Materials Science, Shanghai Dianji University, Shanghai 201306, China*

Corresponding authors: YX02SHU14@shu.edu.cn (X. Yu), xlzou@shu.edu.cn (X. Zou).

1. Experimental section

1.1. Chemicals and reagents

Methylimidazole ($C_4H_6N_2$, 99%), Cobalt nitrate hexahydrate ($Co(NO_3)_2 \cdot 6H_2O$, 98%) were purchased from Shanghai Aladdin Co. Ltd. Thioacetamide (TAA, NA), Potassium hydroxide (KOH, >99%), Methanol (CH_3OH, >99%), Choline chloride [$HOC_2H_4N(CH_3)_3Cl$, 99%] (ChCl) and ethylene glycol [$(CH_2OH)_2$, >99%] (EG) were purchased from Sigma-Aldrich. IrO_2 were purchased from Shanghai Bidd Pharmaceutical Technology Co. Ltd. All chemical reagents were used as received without any further purification.

1.2. Preparation of Co@CN on CC

The as-prepared Co-ZIF precursor was placed at the middle of a porcelain boat, and the porcelain boat was placed in a tubular furnace that was vacuumed twice and then saturated by Ar. Afterwards, the tubular furnace was heated to 800 ℃ with a ramping rate of 2 ℃ min^{-1} and stayed at 800 ℃ for 2 h for carbonizing of Co-ZIF to yield Co@CN.

1.3. Preparation of CoS_2@CN on CC

The as-prepared Co-ZIF precursor was placed at the middle of a porcelain boat, and 2.0 g of TAA placed at the upstream side. The porcelain boat was placed in a tubular furnace that was vacuumed twice and then saturated by Ar. Afterwards, the tubular furnace was heated to 500 ℃ with a ramping rate of 2 ℃ min^{-1} and stayed at 500 ℃ for 2 h for vulcanizing and carbonizing simultaneously of Co-ZIF to yield CoS_2@CN.

1.4. Preparation of benchmark electrode (IrO_2)

For comparison, IrO_2 electrode w*as* fabricated for OER. The 10 mg catalyst powder was dispersed in 400 μL ethanol solution containing 60 μL 5wt% of Nafion solution, and then 140 μL deionized water was added, followed by ultrasonication for 30 minutes to form a homogeneous ink. Then 600 μL of catalyst ink was dropped onto the activated carbon cloth (1 × 1 cm^2). After drying at 90 ℃, the loading amount of IrO_2 catalyst was 5 mg cm^{-2}.

2. OER mechanism

The OER mechanism under alkaline condition included four reaction steps, which is a four-electron transfer process:

$$* + OH^- \rightarrow * OH + e^-$$

$$* OH + OH^- \rightarrow * O + H_2O + e^-$$

$$* + OH^- \rightarrow * OOH + e^-$$

$$* OOH + OH^- \rightarrow * + O_2 + H_2O + e^-$$

The * was the adsorption site, and *OH, *O, and *OOH stood for the OER reaction intermediates.

3. Calculation of turnover frequency (TOF)

TOF (s^{-1}) represents the number of products generated by a single active site per unit time, and the commonly used formula is[S1]:

$$\mathrm{TOF}(s^{-1}) = \frac{j * \mathrm{A}}{\mathrm{z} * \mathrm{F} * \mathrm{n}}$$

Where *j* is the current density under a certain overpotential (mA cm^{-2}),

A is the working electrode area,

z is the electron transfer number of the catalytic reaction,

n is the amount of substance at the active site (mol),

F is Faraday's constant (96485 C mol^{-1}).

A material usually having a metal as the active site[S2]:

TOF = (Number of oxygen molecules)/(Number of active sites) (1)

All bulk phase metal atoms are considered as active sites, applicable to monatomic catalysts[S3]:

Substitute equation n=m*N_1 into (1), we get the following equation:

$$\mathrm{TOF_{Bulk}} * \mathrm{N_1} = \frac{\mathrm{I} * \mathrm{N_A}}{\mathrm{z} * \mathrm{F} * \mathrm{m}}$$

The number of oxygen turnovers is obtained from the current density (*j*)

using the equation:

$$\text{Number of oxygens} = \left(j \frac{\text{mA}}{\text{cm}^2}\right)\left(\frac{1\text{C/s}}{1000\text{ mA}}\right)\left(\frac{1\text{ mole e}^-}{96485.3\text{ C}}\right)\left(\frac{1\text{ mol O}_2}{4\text{ mol e}^-}\right)\left(\frac{6.022\ \text{x}\ 10^{23}\text{ molecules O}_2}{1\text{ mole O}_2}\right)$$

$$= 1.56 \text{ x } 10^{15} \left(\frac{\text{O}_2/\text{s}}{\text{cm}^2}\right) \text{per} \left(\frac{\text{mA}}{\text{cm}^2}\right)$$

The number of Ir ions in CoP_2@CN-Ir(*x*) electrocatalyst is obtained from the ICP-OES. Consequently, the number of Ir sites is:

$$\left(\frac{\omega\text{t.\%(Ir)}}{100\text{ mg}}\right) \times \left(\frac{\text{m(Ir)}}{2\text{ cm}^2}\right) \times \left(\frac{1\text{ mmol}}{192.22\text{ mg}}\right) \times 6.022\ \times 10^{20} \left(\frac{\text{sites}}{\text{mmole}}\right)$$

The number of Co ions in CoP_2@CN-Ir(*x*) electrocatalyst is obtained from the ICP-OES. Consequently, the number of Co sites is:

$$\left(\frac{\omega t.\%(Co)}{100\ mg}\right) \times \left(\frac{m(Co)}{2\ cm^2}\right) \times \left(\frac{1\ mmol}{58.93\ mg}\right) \times 6.022\ \times 10^{20}\ \left(\frac{sites}{mmole}\right)$$

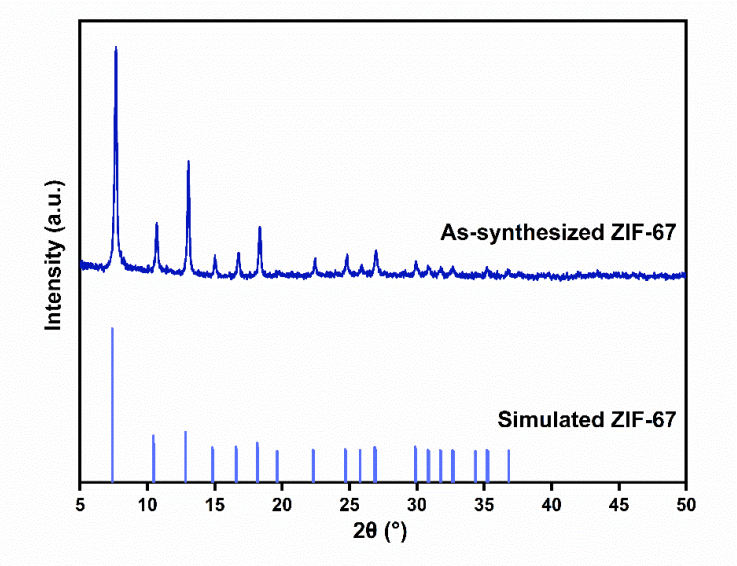

Fig. S1 XRD pattern of Co-ZIF/CC.

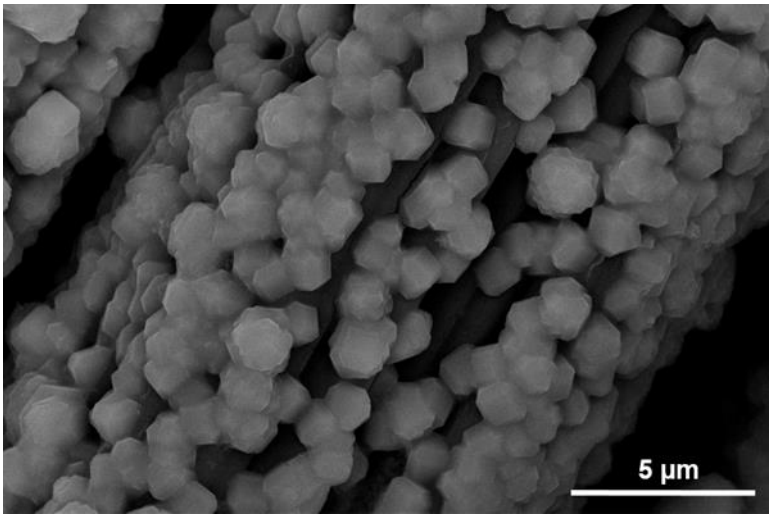

Fig. S2 SEM image of ZIF-67.

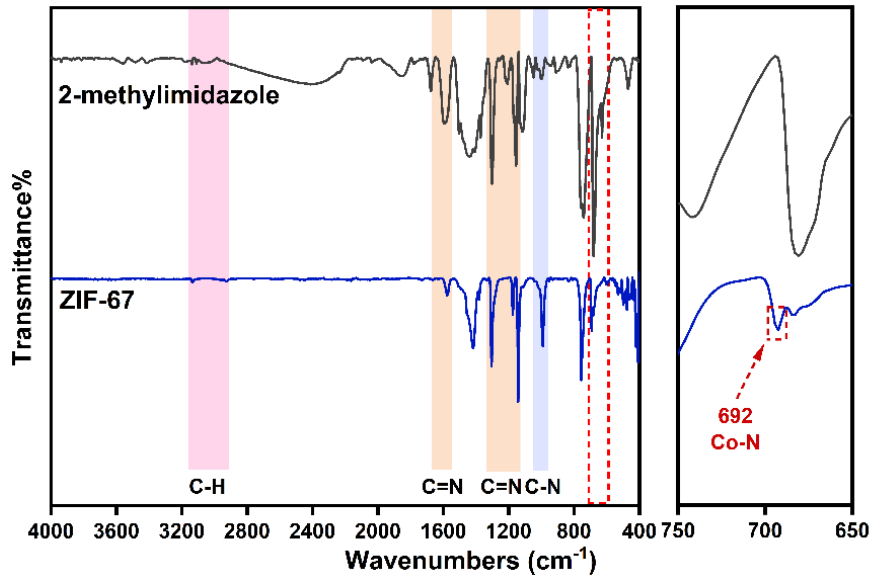

Fig. S3 FTIR spectra of Co-ZIF and 2-methylimidazole.

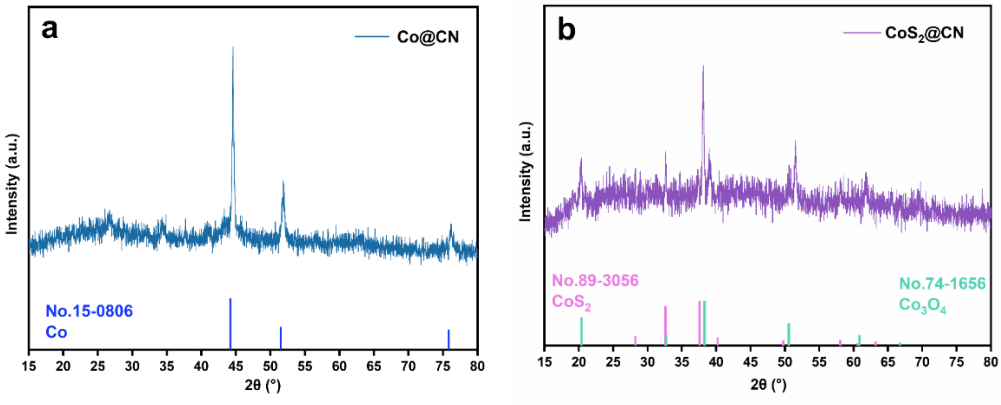

Fig. S4 XRD patterns of (a) Co@CN and (b) CoS_2@CN.

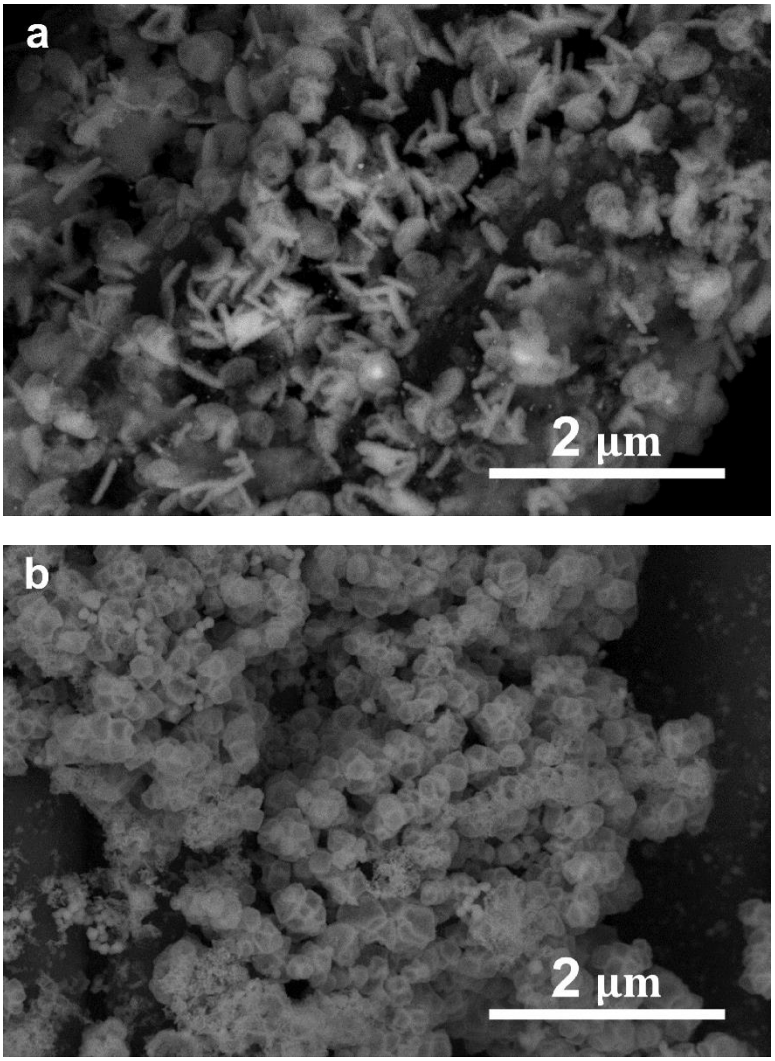

Fig. S5 SEM images of (a) Co@CN and (b) CoS_2@CN.

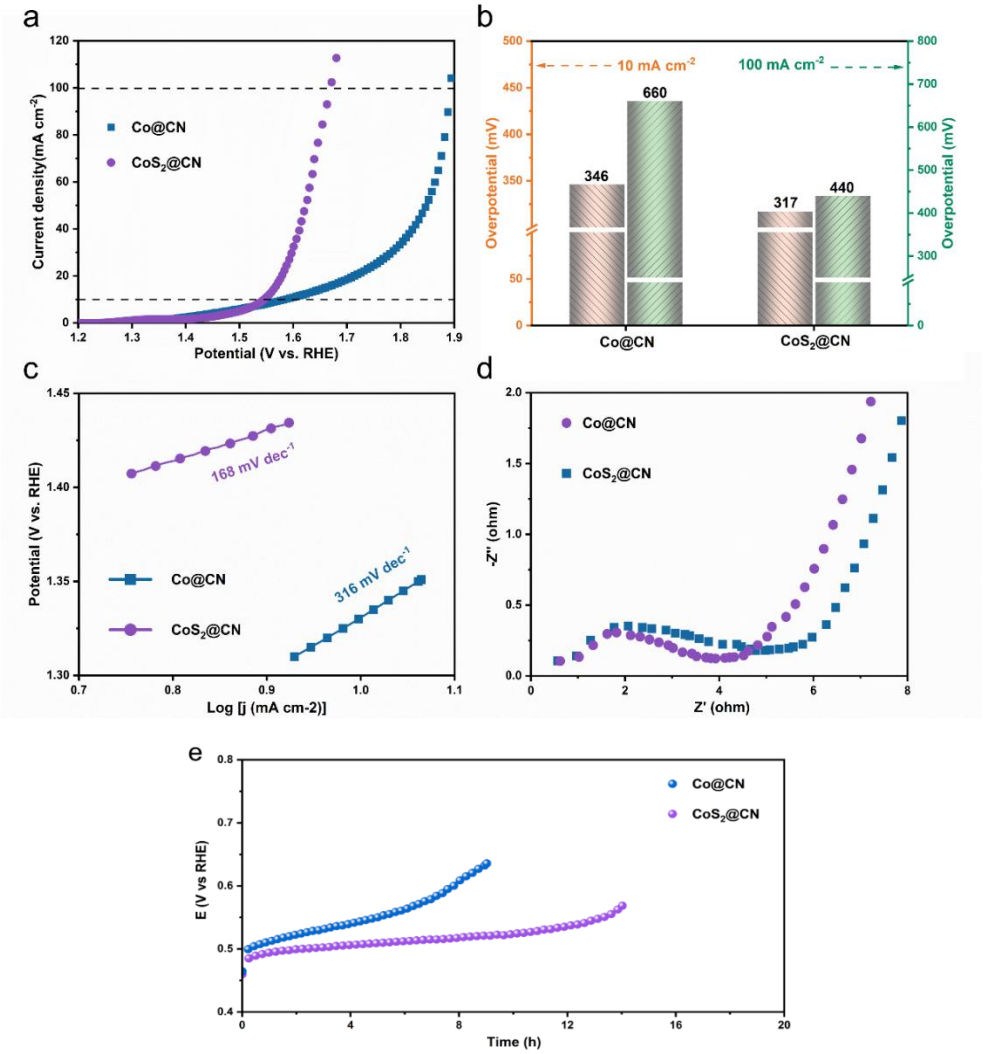

Fig. S6 OER properties of Co@CN and CoS_2@CN. (a) Polarization curves. (b) Overpotentials at 10 mA cm^{-2} and 100 mA cm^{-2}, respectively. (c) Tafel plots. (d) Nyquist plots. (e) The voltage-time curves at 10 mA cm^{-2}.

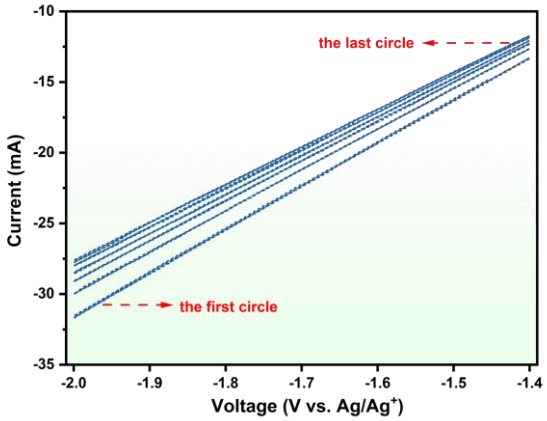

Fig. S7 Selective typical CV curves for depositing Ir atoms.

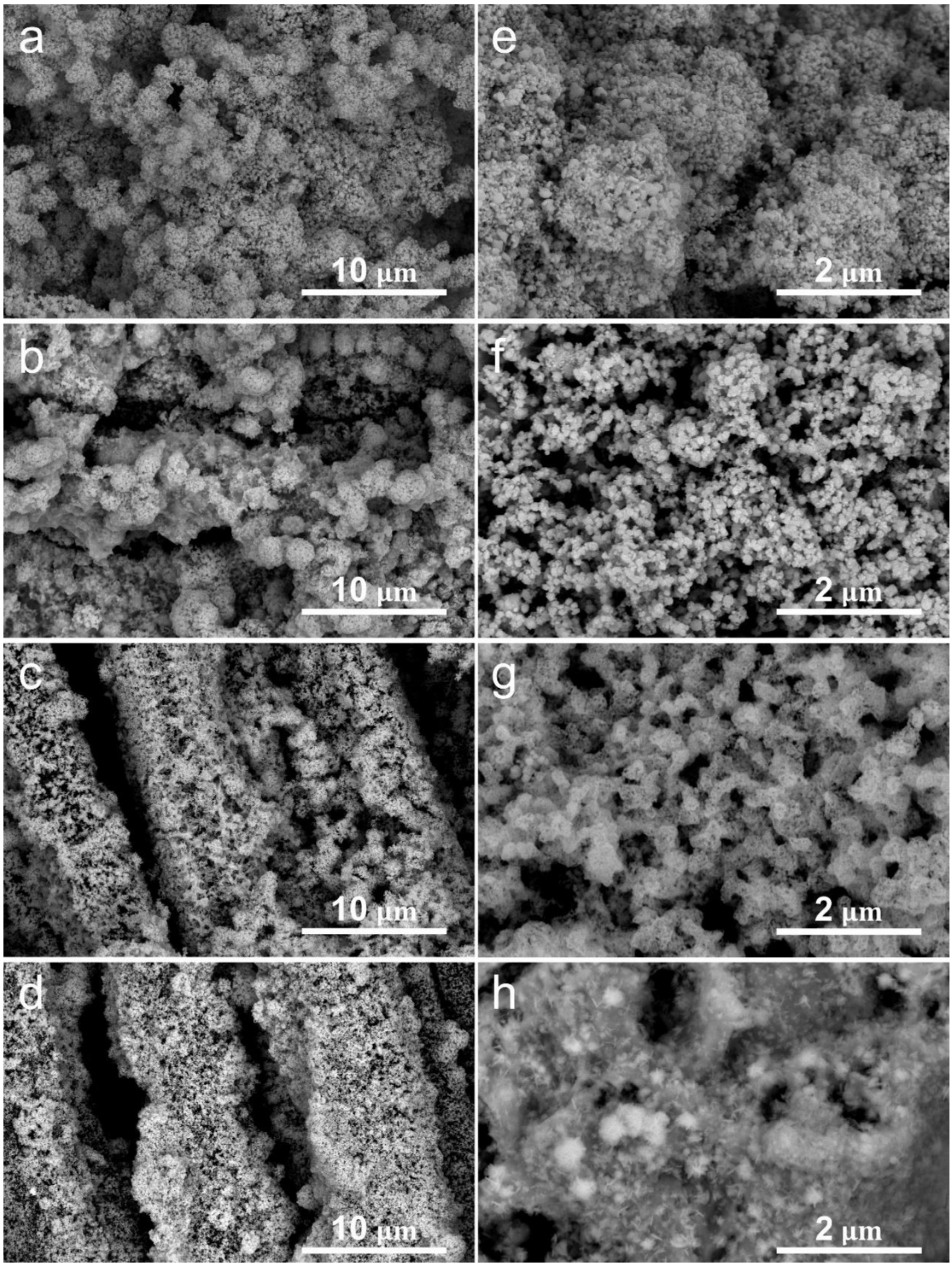

Fig. S8 (a-d) Low and (e-f) high-magnification SEM images of (a, e) CoP_2@CN, (c, f) CoP_2@CN-Ir(100), (c, g) CoP_2@CN-Ir(200) and (d, h) CoP_2@CN-Ir(300).

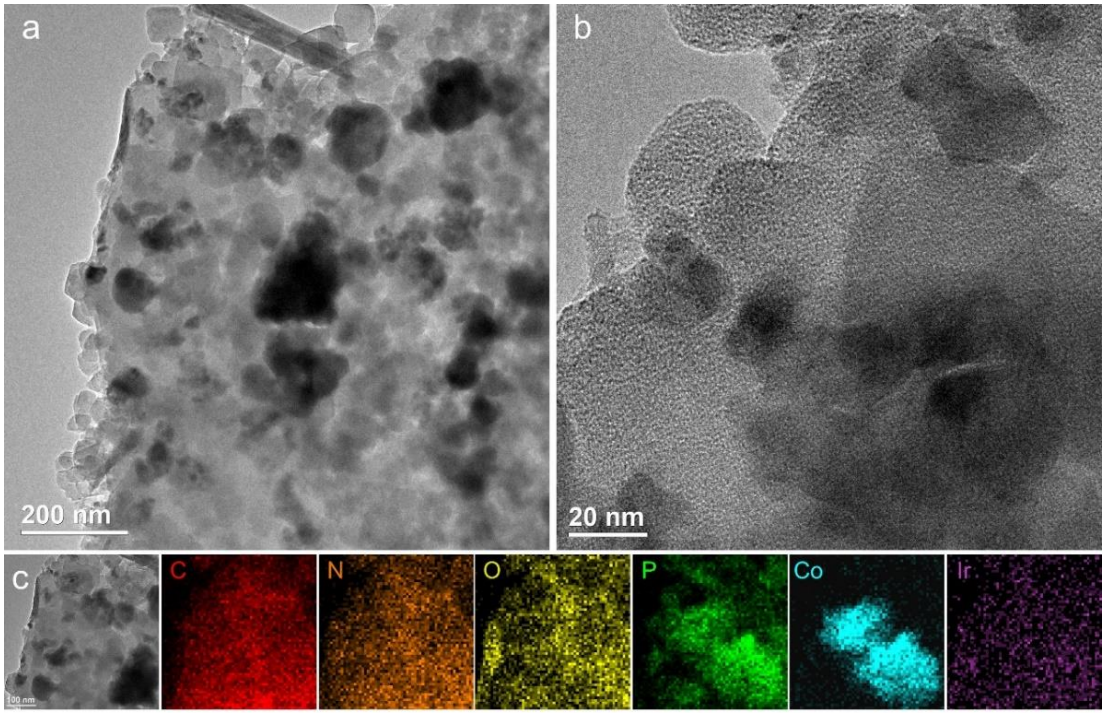

Fig. S9 (a, b) TEM images of CoP_2@CN-Ir(200) at different magnifications and (c) EDS elemental mapping images of C, N, O, P, Co and Ir.

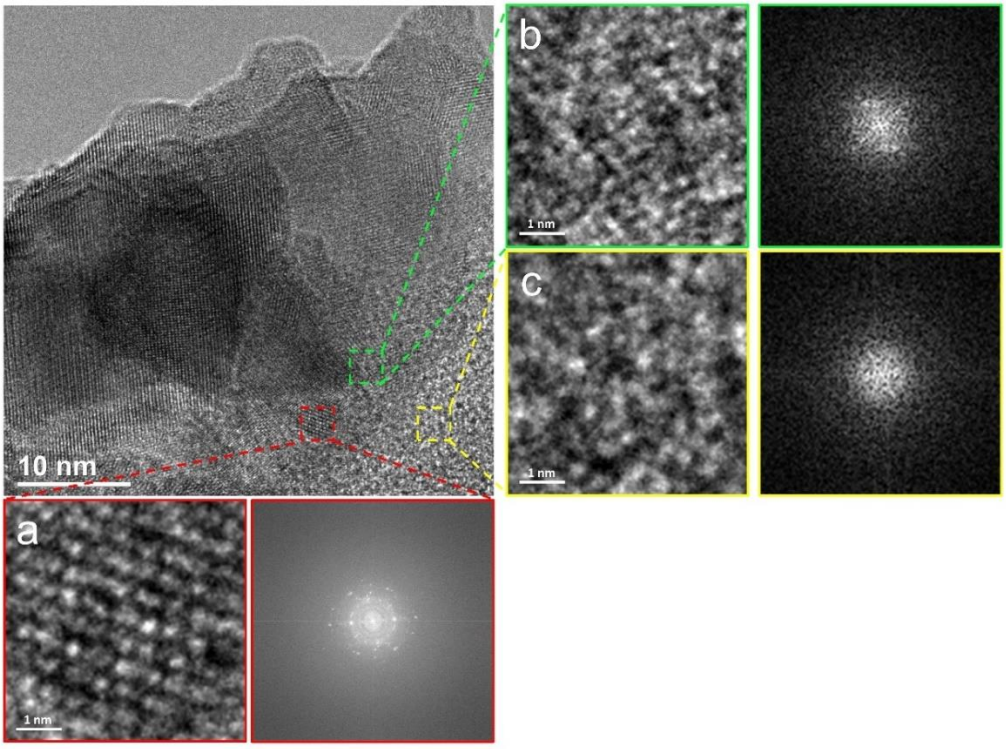

Fig. S10 Enlarged HRTEM images and the corresponding FFT patterns from a same HRTEM image (top left). (a) crystalline CoP_2; (b) amorphous CoO_x; (c) amorphous CN.

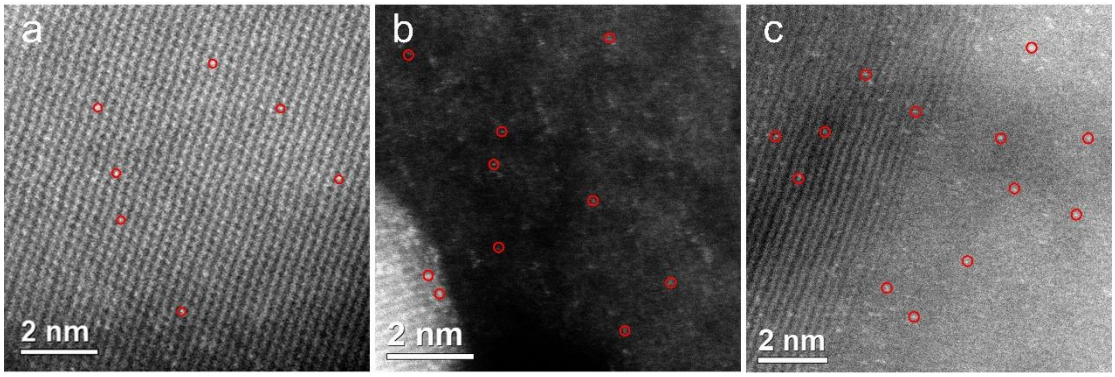

Fig. S11 AC-HAADF-STEM images of CoP_2@CN-Ir(200). (a) Crystalline CoP_2 region; (b) Amorphous CoO_x region; (c) Crystalline CoP_2 and amorphous CoO_x heterogeneous region (Ir single atoms circled in red).

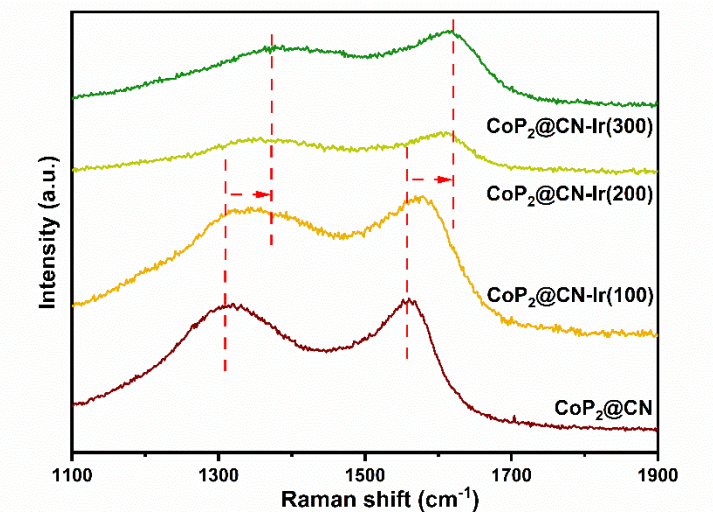

Fig. S12 Local enlarged image of Raman spectra of CoP_2@CN and CoP_2@CN-Ir(x) (1100 cm^{-1} ~ 1900 cm^{-1}).

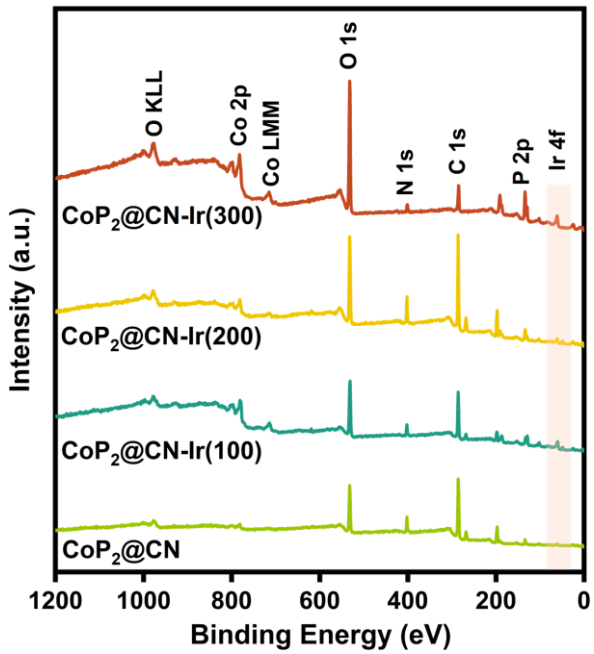

Fig. S13 XPS survey spectra for CoP_2@CN and CoP_2@CN-Ir(*x*).

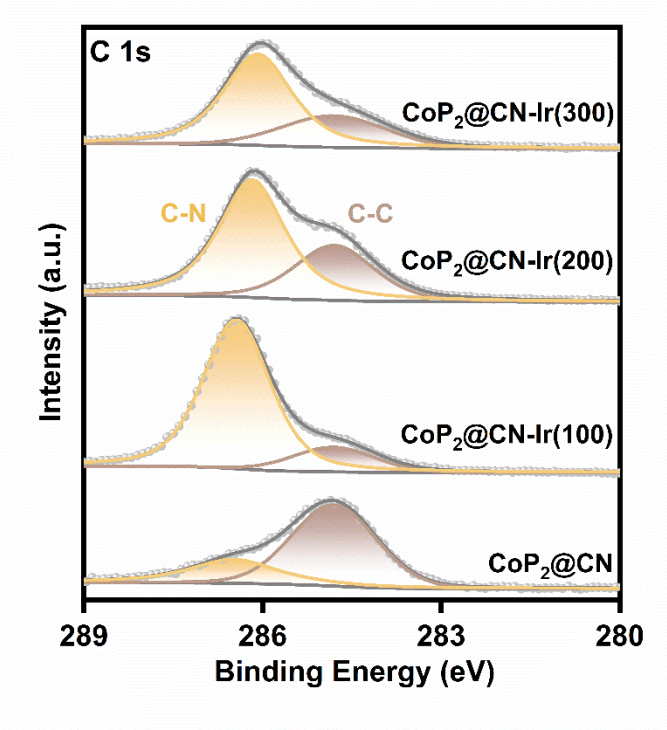

Fig. S14 High-resolution XPS spectra of C 1s.

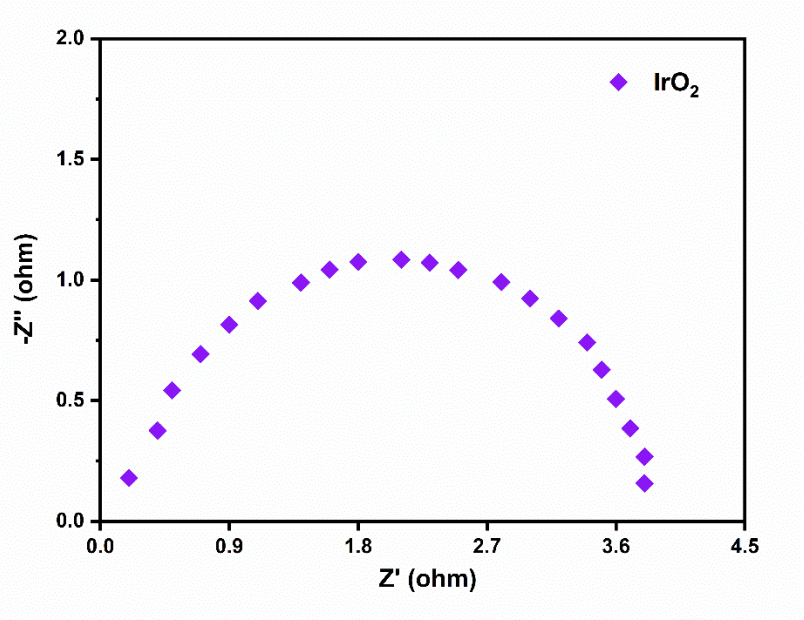

Fig. S15 Nyquist plot of IrO_2.

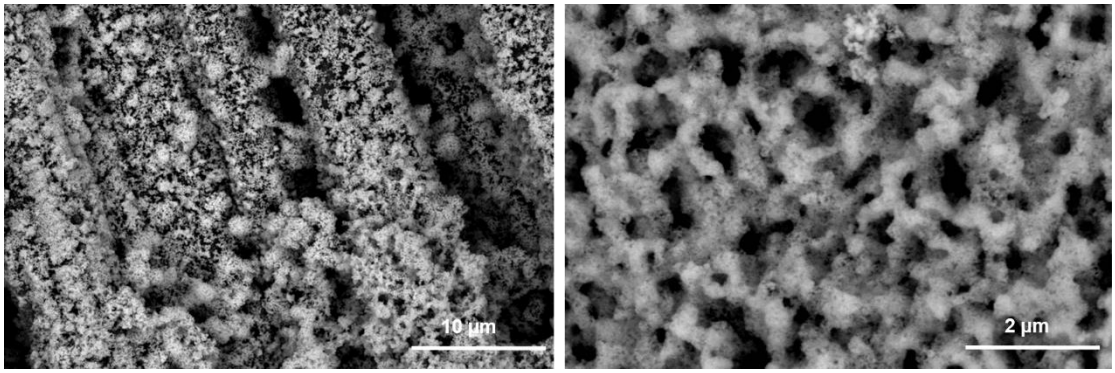

Fig. S16 SEM images of CoP_2@CN-Ir(200) after OER stability test at 10 mA cm^{-2} for 24 h.

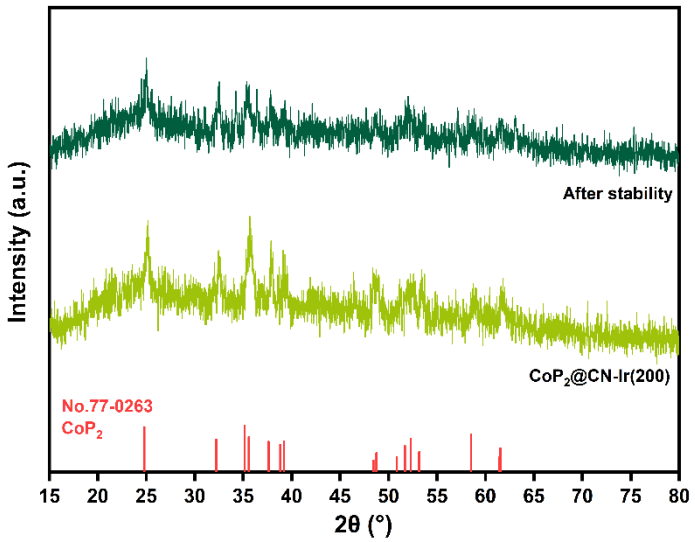

Fig. S17 XRD patterns of CoP_2@CN-Ir(200) after OER stability test at 10 mA cm^{-2} for 24 h.

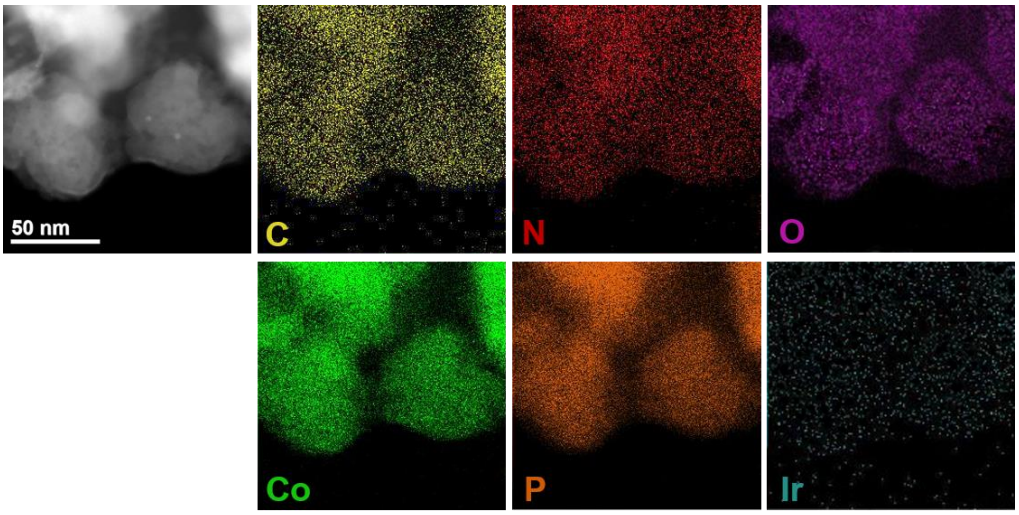

Fig. S18 AC-HAADF-STEM-EDS elemental mapping images of C, N, O, Co, P and Ir after OER stability test at 10 mA cm^{-2} for 24 h.

Table S1. N 1s XPS elemental analysis of CoP_2@CN and CoP_2@CN-Ir(x).

Catalysts	Metal-N	Pyridinc-N	Pyrrolic-N	Graphitic-N
CoP_2@CN	10.29	11.31	48.87	29.53
CoP_2@CN-Ir(100)	7.14	23.81	31.10	30.95
CoP_2@CN-Ir(200)	7.09	21.28	36.17	35.46
CoP_2@CN-Ir(300)	6.89	15.67	38.18	39.16

Table S2. TOF values at different overpotentials (η) for various electrodes assuming the metal atoms are active for OER.

		η (mV)					
	Mol (unit cm^{-2})	190	210	230	270	290	310
IrO_2	1.47×10^{16}	0.40 s^{-1}	0.53 s^{-1}	0.67 s^{-1}	1.03 s^{-1}	1.27 s^{-1}	1.60 s^{-1}
CoP_2@CN	1.31×10^{16}	0.40 s^{-1}	0.44 s^{-1}	0.51 s^{-1}	0.75 s^{-1}	0.97 s^{-1}	1.27 s^{-1}
CoP_2@CN-Ir(100)	1.45×10^{16}	0.40 s^{-1}	0.48 s^{-1}	0.55 s^{-1}	0.78 s^{-1}	1.31 s^{-1}	2.15 s^{-1}
CoP_2@CN-Ir(200)	1.85×10^{16}	0.85 s^{-1}	1.44 s^{-1}	2.24 s^{-1}	6.07 s^{-1}	8.89 s^{-1}	12.53 s^{-1}
CoP_2@CN-Ir(300)	1.97×10^{16}	0.44 s^{-1}	0.97 s^{-1}	1.31 s^{-1}	8.89 s^{-1}	5.04 s^{-1}	7.51 s^{-1}

Table S3. Comparison of OER performance of various electrocatalysts in 1 M KOH electrolyte.

Catalysts	η_{10} (mV)	Tafel slope (mV dec^{-1})	Reference
CoP_2@CN-Ir(200)	**189**	**39**	**This work**
Ir_{SAC}-NiFe-LDH	194	33.3	*ACS Catal.*, 2023, **13**, 11195-11203[S4]
Ir/Ni DHBT	195	44	*ACS Catal.*, 2023, **13**, 1726-1739[S5]
$Ir/Ni_2P_4O_{12}$	186	42.15	*Adv. Funct. Mater.*, 2023, 2309824[S6]
Co-SAC/RuO_2	200	110	*Angew. Chem. Int. Ed.*, 2022, **61**, e202114951[S7]
Ir-$Ni(OH)_2$	260	78	*Nano Lett.*, 2022, **22**, 3832-3839[S8]
Ru_{SAs}/AC-FeCoNi	205	40	*Adv. Energy Mater.*, 2020, **11**, 2002816[S9]
Ir-$Ni(OH)_2$	224	41	*Adv. Mater.*, 2020, **32**, 2000872[S10]
Ir-NiO	215	38	*J. Am. Chem. Soc.*, 2020, **142**, 7425-7433[S11]
Ir_1/Vo-CoOOH	200	32	*Nat. Commun.*, 2022, **13**, 2473[S12]
Co@CN_x	480	239	*Adv. Funct. Mater.*, 2023, **33**, 2300405[S13]
Ir/Ni-Co_3O_4	177	41.3	*Adv. Energy Mater.*, 2023, **13**, 2302537[S14]
Fe/Ni-NC||FeNi@G	273	52.3	*Electrochim. Acta*, 2023, **458**, 142549[S15]
Ir_1/NiCr LDH	232	51	*J. Mater. Chem.*, A 2024, **12**, 2491-2500[S16]
Ir_{25}-$Fe_{16}Ni_{100}P_{64}$	232	48	*Small*, 2023, **19**, 2207253[S17]
Ir_1/Ni LDH-T	228	41	*Nat. Commun.*, 2024, **15**, 559[S18]

Table S4. Comparison of OER performance between CoP_2@CN-Ir(200) and Ni- and/or Co-based double hydroxides in 1 M KOH electrolyte.

Catalysts	η_{10} (mV)	Tafel slope (mV dec^{-1})	Reference
CoP_2@CNIr(200)	**189**	**39**	**This work**
v-NiFe LDH	210	34.8	*Nano Energy*, 2021, **81**, 105606[S19]
CoFe@NiFe200/NF	190	45.71	*Appl. Catal. B Environ.*, 2019, **253**, 131-139[S20]
Mo-NiCo $LDHs_{(Vo)}$	258	94.5	*Chem. Eng. J*, 2023, **463**, 142396[S21]
FCNSNP	349	44.09	*iScience*, 2022, **25**, 105148[S22]
NiFe LDH/GQDs	189	23.6	*Nano Energy*, 2021, **84**, 105932[S23]
B-Co_2Fe LDH	205	39.2	*Nano Energy*, 2021, **83**, 105838[S24]
NiFeCo/NF	195	47.0	*J. Mater. Chem. A*, 2023, **11**, 22941-22950[S25]
$Ni_{0.3}Fe_{0.7}$LDH@NF	184	56.68	*Appl. Catal. B Environ.*, 2023, **323**, 122091[S26]
$Ni_{4/5}Fe_{1/5}$-LDHs-S-2	257	61.5	*Chin. J. Catal.*, 2020, **41**, 847-852[S27]
$Co_1Fe_{0.2}$LDH	256	40.0	*Chin. J. Catal.*, 2022, **43**, 2240-2248[S28]
NiCoFe-HO@NiCo-LDH YSMRs	278	49.7	*ngew. Chem. Int. Ed.*, 2022, **61**, e202213049[S29]

Table S5. Comparison of OER performance of various electrocatalysts in 1 M KOH electrolyte at 100 mA cm^{-2}.

Catalysts	η_{100} (mV)	Tafel slope (mV dec^{-1})	Reference
CoP_2@CN-Ir(200)	**300**	**39**	**This work**
$Ir_{SAC}/Ni(OH)_2$@HP-NF	291	58	*Nano Res.*, 2022, **15**, 10014-10020[S30]
MX@MOF-Co_2P	407	55.20	*ACS Appl. Mater.*, 2024, **16**, 16132-16144[S31]
Co-ZIF/CDs/CC	320	28.18	*J. Mater. Sci. Technol.*, 2023, **145**, 74-82[S32]
CNP@NF	401	147	*Small*, 2023, **19**, 2206723[S33]
Ir-Co_3O_4@NC	341	146.5	*SM&T*, 2022, **33**, e00461[S34]
Fe-NC	525	89	*Chem. Eng. J.*, 2023, **468**, 143717[S35]
CNT-NC-CoP	355	98	*Chem. Eng. J.*, 2023, **455**, 140694[S36]
Co_2P/Ni_2P-2%Mo	377	82.1	*Carbon*, 2019, **141**, 643-651[S37]
Co@N-CS/N-HCP@CC	357	46.1	*Appl. Catal. B Environ.*, 2020, **272**, 118951[S38]

References

S1 W. Chen, B. Wu, Y. Wang, W. Zhou, Y. Li, T. Liu and C. Xie, *Energ Environ. Sci.*, 2021, **14**, 6428-6440.

S2 S. Hao, H. Sheng, M. Liu, *Nat. Nanotechnol.*, 2021, **16**, 1371-1377.

S3 A. Sengeni, K. Pitchiah, N. Suguru, *Angew. Chem. Int. Ed. Engl.*, 2021, **60**, 23051-23067.

S4 Y. Hu, T. Y. Shen, Z. Song, Z. Wu, S. Bai, G. Liu, X. Sun, *ACS Catal.*, 2023, **13**, 11195-11203.

S5 M. H. Hao, B. Assresahegn, A. Abdellah, L. Miner, A. Hejami, *ACS Catal.*, 2023, **13**, 1726−1739.

S6 X. Liu, S. Jing, K. Wang, C. Ban, J. Ding, Y. Feng, Y. Duan, *Adv. Funct. Mater.*, 2023, 2309824.

S7 K. Shah, R. Dai, M. Mateen, Z. Hassan, Z. Zhuang, C. Liu, M. Israr, W. C. Cheong, B. Hu, R. Tu, C. Zhang, X. Chen, Q. Peng, C. Chen, Y. Li, *Angew. Chem. Int. Ed.*, 2022, **61**, e202114951.

S8 Q. He, S. Qiao, Q. Zhou, Y. Zhou, H. Shou, P. Zhang, W. Xu, D. Liu, S. Chen, X. Wu, L. Song, *Nano Lett.*, 2022, **22**, 3832-3839.

S9 Y. Hu, G. Luo, L. Wang, X. Liu, Y. Qu, Y. Zhou, F. Zhou, Z. Li, Y. Li, T. Yao, C. Xiong, B. Yang, Z. Yu, Y. Wu, Single Ru stoms stabilized by hybrid amorphous/crystalline FeCoNi layered double hydroxide for ultraefficient oxygen evolution, *Adv. Energy Mater.*, 2020, **11**, 2002816.

S10 G. Zhao, P. Li, N. Cheng, S. Dou, W. Sun, An Ir/$Ni(OH)_2$ heterostructured electrocatalyst for the oxygen evolution reaction: breaking the scaling relation, stabilizing rridium(V), and beyond, *Adv. Mater.*, 2020, **32**, 2000872.

S11 Q. Wang, X. Huang, Z. Zhao, M. Wang, B. Xiang, J. Li, Z. Feng, H. Xu, M. Gu, J. Am, *J. Am. Chem. Soc.*, 2020, **142**, 7425-7433.

S12 Z. Zhang, C. Feng, D. Wang, S. Zhou, R. Wang, S. Hu, H. Li, M. Zuo, Y. Kong, J. Bao, J. Zeng, *Nat. Commun.*, 2022, **13**, 2473.

S13 Q. Javier, G. Sergio, D. Ayoub, Z.Andrea, *Adv. Funct. Mater.*, 2023, **33**, 2300405.

S14 A. Wang, W. Wang, J. Xu, A. Zhu, C. Zhao, M. Yu, *Adv. Energy Mater.*, 2023, **13**, 2302537.

S15 Z. Xu, G. Chen, F. Yang, J. Jan, G. Liu, F. Xiao, Y. Sun, X. Qiu, *Electrochim. Acta*, 2023, **458**, 142549.

S16 Swayamprakash Biswal, Divya, Biswajit Mishra, Darius Pohl, Bernd Rellinghaus, *J. Mater. Chem. A*, 2024, **12**, 2491–2500.

S17 N. Yang, S. Tian, Y. Feng, Z. Hu, H. Liu, *Small*, 2023, **19**, 2207253.

S18 J. Wei, H. Tang, L. Sheng, R. Wang, M. Fan, J. Wan, Y. Wu, *Nat. Commun.*, 2024, **15**, 559.

S19 Y. Wang, S. Tao, H. Lin, G. Wang, K. Zhao, R. Cai, K. Tao, C. Zhang, M. Sun, J. Hu, B. Huang, *Nano Energy*, 2021, **81**,105606.

S20 R. Yang, Y. Zhou, Y. Xing, D. Li, D. Jiang, M. Chen, W. Shi, S. Yuan, *Appl. Catal. B Environ.*, 2019, **253**,131-139.

S21 K. Chen, Y. H. Cao, S. Yadav, Kim GC, Z. Han, W. Wang, W. J. Zhang, V. Dao, I H Lee, *Chem. Eng. J*, 2023, **463**, 142396.

S22 M. B. Z. Hegazy, K. Harrath, D. Tetzlaff, M. Smialkowski, D. Siegmund, D. Siegmund, J. Li, R. Cao, U. Apfel, Boosting the overall electrochemical water splitting performance of pentlandites through non-metallic heteroatom incorporation, *iScience*, **25**, 105148.

S23 X. Guo, X. Zheng, X. Hu, Q. Zhao, L. Li, P. Yu, C. Jing, Y. Zhang, G. Huang, B. Jiang, C. Xu, F. Pan, *Nano Energy*, 2021, **84**, 105932.

S24 L. Wu, L. Yu, Q. Zhu, B. McElhenny, F. Zhang, C. Wu, X. Xing, J. Bao, S. Chen, Z. Ren, *Nano Energy*, **83**, 105838.

S25 J. Z. Soo, A. Riaz, F. Kremer, F. Brink, C. Jagadish, H. H. Tan, S. Karuturi, *J. Mater. Chem. A*, 2023, **11**, 22941-22950.

S26 Y. Zhai, X. Ren, Y. Sun, D. Li, B. Wang, S. F. Liu, *Appl. Catal. B Environ.*, 2023, **323**, 122091.

S27 S. Li, J. Liu, S. Duan, T. Wang, Q. Li, *Chin. J. Catal.*, 2020, **41**, 847-852.

S28 X. Bai, Z. Duan, B. Nan, L. Wang, T. Tang, J. Guan, *Chin. J. Catal.*, 2022, **43**, 2240-2248.

S29 Q. Niu, M. Yang, D. Luan, N. W. Li, L. Yu, X. W. Lou, *Angew. Chem. Int. Ed.*, 2022, **61**, e202213049.

S30 C. Jia, H. Qin, C. Zhen, H. Zhu, Y. Yang, A. Han, L. Wang, G. Liu, H. M. Cheng, *Nano Res.*, 2022, **15**, 10014-10020.

S31 M. Y. Yu, Y. F. Yao, K. Fang, L. S. Chen, L. P. Si, H. Y. Liu, *ACS Appl. Mater.*, 2024, **16**, 16132-16144.

S32 J. Li, C. Chen, Z. Lv, W. Ma, M. Wang, Q. Li, J. Dang, *J. Mater. Sci. Technol.*, 2023, **145**, 74-82.

S33 Q. Hong, Y. Wang, R. Wang, Z. Chen, H. Yang, K. Yu, Y. Liu, H. Huang, Z. Kang, P. W. Menezes, *Small*, 2023, **19**, 2206723.

S34 Y. Zhang, H. Liu, R. Ge, J. Yang, S. Li, Y. Liu, W. Li, *SM&T*, 2022, **33**, e00461.

S35 S. Jung, R. A. Senthil, C. J. Moon, N. Tarasenka, A. Min, S. J. Lee, M. Y. Choi, *Chem. Eng. J.*, 2023, **468**, 143717.

S36 X. Yang, J. Cheng, X. Yang, Y. Xu, H. Li, W. Sun, J. Zhou, *Chem. Eng. J.*, 2023, **455**, 140694.

S37 X. Wang, Z. Ma, L. Chai, L. Xu, Z. Zhu, Y. Hu, S. Huang, *Carbon*, 2019, **141**, 643-651.

S38 H. Liu, M. Jin, D. Zhan, J. Wang, X. Cai, Y. Qiu, L. Lai, *Appl. Catal. B Environ.*, 2020, **272**, 118951.

S39 Z. Chen, Y. Ha, H. Jia, X. Yan, M. Chen, M. Liu, R. Wu, *Adv. Energy Mater.*,2019, **9**, 1803918.